Available online at www.sciencedirect.com

ScienceDirect

Proceedings of the Combustion Institute 39 (2023) 2169–2178

Proceedings of the Combustion Institute

www.elsevier.com/locate/proci

Turbulent kinetic energy evolution in turbulent boundary layers during head-on interaction of premixed flames with inert walls for different thermal boundary conditions

Sanjeev Kr. Ghai [a,*], Umair Ahmed [a], Markus Klein [b], Nilanjan Chakraborty [a]

[a] *School of Engineering, Newcastle University, Claremont Road, Newcastle Upon Tyne NE1 7RU, UK*
[b] *Department of Aerospace Engineering, LRT1, University of the Bundeswehr Munich, Werner-Heisenberg-Weg 39, Neubiberg 85577, Germany*

Received 4 January 2022; accepted 23 August 2022
Available online 21 October 2022

Abstract

The statistical behaviour of turbulent kinetic energy, and its transport in turbulent boundary layers during premixed flame-wall interaction for isothermal and adiabatic chemically inert walls have been analysed using a Direct Numerical Simulation (DNS) database. The terms due to the mean velocity gradient (commonly known as the production term) and viscous dissipation remain leading order contributors to the turbulent kinetic energy transport when the flame is away from the wall, similar to that in the corresponding non-reacting turbulent boundary layer, but in addition to these terms, the pressure dilatation and pressure transport contributions play leading order roles when the flame interacts with the wall. It has been found that the gradient hypothesis-based Reynolds stress closures in the context of the $k-\varepsilon$ model may yield an inaccurate prediction of the mean velocity gradient term due to the counter-gradient behaviour of Reynolds stresses in the premixed flame cases considered in this analysis. The thermal boundary condition at the wall does not have a major influence apart from a higher wall friction velocity for adiabatic boundary condition than in the case of isothermal boundary condition. The assumption of local equilibrium of production and dissipation of turbulent kinetic energy has been found to be rendered invalid when the flame is either near to the wall or interacting with the wall. This invalidates the conventional log-law for mean streamwise velocity variation, and the wall functions derived based on production-dissipation balance equipped by the usual gradient hypothesis in the context of the standard $k-\varepsilon$ model for premixed flame-wall interaction in turbulent boundary

* Corresponding author.
E-mail address: sanjeev.ghai@newcastle.ac.uk (S.Kr. Ghai).

https://doi.org/10.1016/j.proci.2022.08.055

layers. Therefore, improved wall functions are necessary for Reynolds averaged Navier-Stokes simulations of premixed flame-wall interaction in turbulent boundary layers.

Keywords: Turbulent kinetic energy; Turbulent boundary layer; Premixed flame-wall interaction; Direct numerical simulations (DNS)

1. Introduction

Turbulent kinetic energy (TKE) transport is of fundamental importance in modelling of turbulent flows. However, limited information is available regarding the transport of TKE in the near-wall region during flame-wall interaction (FWI) of premixed flames in turbulent boundary layers (TBLs) [1,2]. In the case of turbulent premixed FWI, the thermal expansion induced by the flame due to the chemical heat release significantly alters the temperature and velocity distributions within TBLs. Therefore, the modelling of TKE transport needs additional consideration due to the turbulence generated by the flame front. Reynolds-Averaged Navier Stokes (RANS) simulations are still predominantly used for industrial computations. In RANS, the non-linear convective term gives rise to the unknown Reynolds stress term which requires modelling. The well-known two-equation $k-\varepsilon$ model is widely used for the closure of Reynolds stresses due to its reasonable range of applicability, robustness and moderate computational overhead [3]. In the $k-\varepsilon$ model, the turbulent eddy viscosity is calculated based on TKE and its dissipation rate. Karlovitz et al. [4] were the first to hypothesise the flame generated turbulence in premixed flames, and Bray and Libby [5] analytically linked this effect to the mean velocity gradient due to the flame normal acceleration which was subsequently confirmed in experiments [6–8].

The advancements in computational power enabled Direct Numerical Simulation (DNS) data to be used for analysing TKE transport for turbulent premixed combustion [1,2,9–11]. Zhang and Rutland [9] used DNS data to model the pressure dilatation and pressure transport contributions to the TKE transport in turbulent premixed combustion. Nishiki et al. [12] proposed models for the unclosed terms of the TKE transport equation based on a-priori analysis of DNS data belonging to the corrugated flamelets regime [13]. Chakraborty et al. [10,11] analysed the statistical behaviour of TKE transport using DNS data, and proposed models for the unclosed terms in different regimes of turbulent premixed combustion and different effective Lewis numbers. However, most of the aforementioned analyses on TKE transport for reacting flows [9–11] were conducted in the absence of walls. Lai et al. [2] investigated the statistical behaviour of the transport of TKE for head-on quenching of statistically planar turbulent premixed flames under the influence of decaying isotropic turbulence for different Lewis numbers. Recently, Ahmed et al. [1] analysed the statistical behaviour of TKE evolution in boundary layer flashback of turbulent H_2-air premixed flames. The main objectives of the present study are (i) to identify the qualitative differences in the TKE transport near and away from the wall for different wall boundary conditions during FWI of premixed flames within TBLs and its implications on the laws of the wall, and (ii) to assess the validity of the assumptions that are usually invoked for the derivation of wall functions for the simulation of non-reacting (NR) TBLs in the context of standard $k-\varepsilon$ modelling in the case of premixed FWI. To meet these objectives, a three-dimensional DNS database of head-on interaction (HOI) of statistically planar flames propagating across TBLs towards a chemically inert walls has been considered for isothermal (I) and adiabatic (A) wall boundary conditions.

2. Mathematical background

The exact equation for the Favre averaged TKE $\widetilde{k}=\overline{\rho u_i'' u_i''}/2\overline{\rho}$ is given by [9]:

$$\frac{\partial(\overline{\rho}\widetilde{k})}{\partial t}+\frac{\partial(\overline{\rho}\widetilde{u}_j\widetilde{k})}{\partial x_j}=\underbrace{-\overline{\rho u_i'' u_j''}\frac{\partial\widetilde{u}_i}{\partial x_j}}_{T_1}\underbrace{-\overline{u_i''}\frac{\partial\overline{p}}{\partial x_i}}_{T_2}+\underbrace{\overline{p'\frac{\partial u_k''}{\partial x_k}}}_{T_3}+\underbrace{\overline{u_i''\frac{\partial\tau_{ij}}{\partial x_j}}}_{T_4}\underbrace{-\frac{\partial\overline{(p'u_i'')}}{\partial x_i}}_{T_5}\underbrace{-\frac{\partial}{\partial x_i}\overline{(\frac{1}{2}\rho u_i'' u_k'' u_k'')}}_{T_6} \quad (1)$$

where u_j is the j^{th} component of velocity and $\tau_{ij}=\mu(\partial u_i/\partial x_j+\partial u_j/\partial x_i)-(2/3)\mu\delta_{ij}(\partial u_k/\partial x_k)$ is the viscous stress tensor in which μ is the dynamic viscosity. Here, $\overline{q}$, $\widetilde{q}=\overline{\rho q}/\overline{\rho}$, $q''=q-\widetilde{q}$ represent Reynolds average, Favre-average and Favre fluctuations of a general quantity q, respectively. The

terms on the right-hand side of the Eq. (1) are the (i) mean velocity gradient (commonly known as the production term), (ii) mean pressure gradient, (iii) pressure dilatation, (iv) combined effect of viscous dissipation and molecular diffusion, (v) pressure transport, (vi) turbulent transport contributions [9,12]. It is worth noting that the terms T_1 to T_6 are unclosed and need modelling in the context of $k-\varepsilon$ modelling framework. However, the production term T_2, is already closed in the context of second-moment closure where the Reynolds stress tensor $-\overline{\rho u_i'' u_j''}$ is modelled using a gradient diffusion hypothesis, or separate transport equations must be solved for each term of the Reynold stress tensor. In this work, the statistical behaviours of the terms T_1 to T_6 of the turbulent kinetic energy transport equation, both in the near-wall region and away from the wall, are analysed based on a three-dimensional DNS database of HOI of statistically planar flames propagating across TBLs towards a chemically inert wall for isothermal and adiabatic wall boundary conditions.

3. DNS Database

The simulations for this work are performed using a well-known compressible three-dimensional DNS code called SENGA+, where the spatial derivatives are evaluated using a 10th order finite difference central scheme for the internal grid points, whereas the order of accuracy gradually reduces to second order for the non-periodic boundaries. A third-order Runge-Kutta scheme is employed for time advancement. Further details on the code are available in [2,10,11,14–16]. For the current analysis, low Mach number flow conditions are considered and the combustion chemistry is represented by a single-step Arrhenius type chemical reaction (a unit mass of Fuel + s unit mass of Oxidiser $\rightarrow (1+s)$ unit mass of Products, where s is the stoichiometric oxidiser-fuel mass ratio) for the sake of computational economy. Several previous analyses [14,15,17,18] used single-step chemistry for the analysis of turbulent premixed FWI, and the same approach has been adopted in this analysis. It has been demonstrated and discussed elsewhere [14,15] that the statistics of reactive scalar gradient, wall heat flux magnitude and the flame quenching distance obtained from a detailed chemical mechanism can be captured accurately, even for single-step chemistry. The current analysis focuses on the fluid dynamical aspect of turbulent combustion, and the chemical reaction rate effects indirectly influence the TKE transport through density and dilatation rate. Thus, the simplification of chemistry is unlikely to affect the conclusions of this analysis. In the simulations a stoichiometric methane-air mixture (i.e. $s=4.0$) under atmospheric conditions is considered. The Lewis number of all the species is taken to be unity and the unburned gas temperature T_R is taken to be $730K$, which yields a heat release rate parameter of $\tau=(T_{ad}-T_R)/T_R=2.3$; where T_{ad} is the adiabatic flame temperature. Standard values are taken for the Prandtl number and the ratio of specific heats (i.e., $Pr=0.7$, $\gamma=1.4$).

In this configuration, the initial flow conditions in the TBL have been generated by a non-reacting turbulent channel flow solution corresponding to $Re_\tau=(\rho_R u_{\tau,NR}h)/\mu_R=110$ where ρ_R is the unburned gas density, μ_R is the unburned gas viscosity and h is the channel half height corresponding to the non-reacting fully developed channel flow solution. The computational domain size for the current analysis is taken to be $10.69h\times 1.33h\times 4h$ with an equidistant grid resolution of $1920\times 240\times 720$, which ensures at least 8 grid points within the thermal flame thickness $\delta_{th}=(T_{ad}-T_R)/max|\nabla T|_L$ (where T is the instantaneous dimensional temperature). This grid resolution is consistent with several previous DNS analyses [9,10,12], which contributed significantly to the TKE transport in turbulent premixed flames. This grid spacing also ensures that $y^+_{NR}=\rho_w u_{\tau,NR}y/\mu_w$ for the wall adjacent grid point remains approximately 0.6 (i.e. $y^+_{NR}\leq 0.6$) where subscript w is used for the values at the wall and $u_{\tau,NR}=\sqrt{|\tau_{w,NR}|/\rho}$ and $\tau_{w,NR}$ are the friction velocity and wall shear stress for the non-reacting channel flow, respectively. In the current simulations, the choice of $1.33h$ is made so that the flame remains away from the outflow boundary and the data from the full channel flow up to $1.33h$ is used to initialise the flow field. Note that the flow field in this region does not affect the flame behaviour as the turbulence fluctuation in boundary layers is highest near the wall and decreases away from the wall. The non-reacting channel flow results are found to be in excellent agreement with previous findings [19] and interested readers are referred to [16,20] for further information regarding the validation of the non-reacting turbulent channel flow solution. In the simulations, $S_L/u_{\tau,NR}$ is taken to be 0.7 and the friction velocity based Mach number $u_{\tau,NR}/a_R=3\times 10^{-3}$ where S_L and a_R are the unstretched laminar burning velocity and acoustic speed in unburned reactants, respectively. For the channel flow configuration, the root-mean square turbulent velocity fluctuation u' scales with $u_{\tau,NR}$ and the longitudinal integral length scale L_{11} scales with h [21], which yield a Damköhler number $Da=L_{11}S_L/u'\delta_{th}$ of 15.80 and a Karlovitz number $Ka=(u'/S_L)^{3/2}(L_{11}/\delta_{th})^{-1/2}$ of 0.36, which are representative of the corrugated flamelets regime combustion [13].

For these simulations, periodic boundary conditions are imposed for the streamwise (i.e. x) and spanwise (i.e. z) directions and the pressure gradient (i.e., $-\partial p/\partial x=\rho u^2_{\tau,NR}/h$) has been imposed in the streamwise flow direction. In the wall-normal direction (i.e. y), a no-slip boundary condition is

implemented at $y = 0$, whereas a Dirichlet boundary condition is specified (i.e., $T_w = T_R$) for the isothermal wall. However, a Neumann boundary condition, given by $\partial T/\partial y = 0$, is used for the adiabatic wall. Note that the unburned gas and wall temperature of $730K$ is consistent with the earlier works [1,22,23] where it is argued that that this temperature is representative of the combustion air delivered by the compression stage in large, stationary gas turbines for power generation. A partially non-reflecting boundary is specified at $y/h = 1.33$ following an improved Navier-Stokes Characteristics Boundary Conditions strategy [24]. In the current simulation setup, the solution from the $1D$ laminar flame simulation is interpolated to the $3D$ grid in such a manner that, the reaction progress variable $c = 0.5$ at $y/h \approx 0.85$, where the reaction progress variable, c is defined based on the fuel mass fraction Y_F as: $c = (Y_{FR} - Y_F)/(Y_{FR} - Y_{FP})$. The subscripts R and P represent the fresh reactant and fully burned products, respectively. The reacting scalar field is initialised in such a manner that the reactant side of the flame faces the wall, whereas the product side of the flame is always facing towards the outflow side of the boundary in the y direction. It should be recognised here that the domain in the wall-normal direction above h is not relevant for the analysis of the data as $c = 0.5$ is initially situated at $0.85h$. The flow configuration used in the present work is similar to the configuration used in the earlier work of Bruneaux et al. [17,18]. However, in the current simulations, the variation of density due to temperature change and an outflow boundary condition are implemented to avoid any change in the thermodynamic pressure due to density variation caused by combustion. During the simulations, the flame propagates and moves towards the wall and interacts with it, and the simulations are conducted until the flame quenches/extinguishes which corresponds to 2.0 flow through times based on the maximum axial mean velocity (i.e. 21.30 $u_{\tau,NR}$). Note that the TBL does not evolve significantly during the course of the simulation [16]. The Reynolds and Favre averaged quantities involving correlations of Reynolds and Favre fluctuations have been calculated by spatial averaging the quantities of interest in the periodic directions (i.e. $x - z$ planes) for a given time instant. This averaging procedure is consistent with the usual practice for temporally evolving shear layers [25,26] or temporally evolving flames in channel flows [17,18]. Furthermore, this way of Favre-averaging does not influence the conclusions of this paper, as it is representative of the RANS/URANS simulation results at the corresponding time.

4. Results and discussions

Fig. 1 shows the instantaneous flame structures represented by the $c = 0.5$ isosurface along with

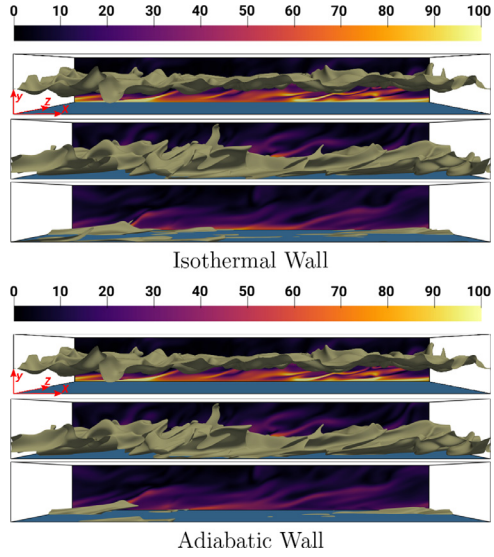

Fig. 1. HOI at $t/t_f = 4.20$, 10.50, and 14.70 (top to bottom) for isothermal (I) and adiabatic (A) wall boundary conditions. The isosurface coloured in grey represents $c = 0.5$. The instantaneous normalised vorticity magnitude Ω is shown on the $x - y$ plane at $z/h = 4$. The blue surface denotes the wall.

the normalised vorticity magnitude, $\Omega = \sqrt{\omega_i\omega_i} \times h/u_{\tau,NR}$ on the $x - y$ plane at $z/h = 4$ for both I and A wall boundary conditions. The time instant $t/t_f = 4.20$ (where $t_f = \delta_{th}/S_L$ is the chemical timescale) exemplifies the situation when the flame is sufficiently away from the wall, and the presence of the wall does not affect the flame propagation. At $t/t_f = 10.50$, the near-wall flow structures such as wall ejections wrinkle the flame surface and therefore alter its location with respect to the wall, which, in turn, affects the flow dynamics, including the TKE transport due to thermal expansion arising from the heat release within the flame. The flame surface starts to interact with the wall surface at $t/t_f = 10.50$ and in the case of I wall boundary condition the flame eventually quenches (e.g. exemplified by the time instant $t/t_f = 14.70$) due to the heat loss through the wall. By contrast, the flame propagates towards the wall and eventually extinguishes (e.g. $t/t_f = 14.70$) once the reactants are completely consumed in the case of A boundary condition. The results shown in Fig. 1 and subsequent figures for an intermediate time instant (i.e. $t/t_f = 12.60$) are shown in the supplementary material but the results shown in the supplementary material follow the same trend with the progress of time as shown in the results presented in the main body of the paper.

The variations of $\widetilde{k}$ in the wall-normal direction at different time instants for FWI in both wall boundary conditions are shown in Fig. 2 along with the corresponding variation obtained for a non-

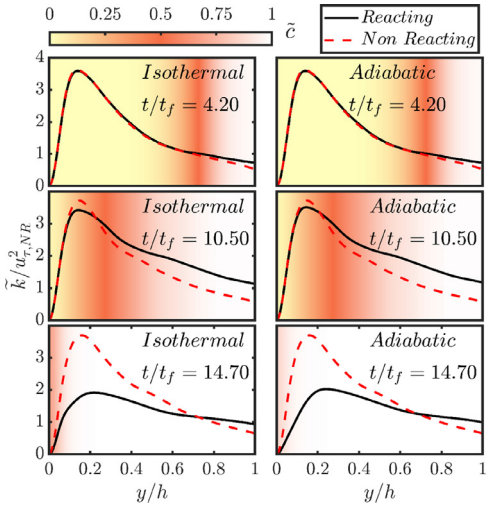

Fig. 2. The variation of $\widetilde{k}/u^2_{\tau,NR}$ with y/h at $t/t_f =$ 4.20, 10.50, and 14.70 for I (left) and A (right) wall boundary conditions. The background is coloured by the values of $\widetilde{c}$ in this and subsequent figures.

reacting flow simulation in this configuration. The background of Fig. 2 and subsequent figures is coloured by the local values of $\widetilde{c}$, which allows for the identification of the position of the flame brush. Fig. 2 shows that the flame brush propagates towards the wall as time progresses and in the case of adiabatic wall the flame eventually extinguishes due to complete consumption of the reactants, which is depicted by the values of $\widetilde{c} \approx 1.0$ at later times of FWI (e.g. at $t/t_f = 14.70$). By contrast, the flame quenches in the vicinity of the wall (e.g. the smallest quenching distance is found to be $1.71\alpha_{T_0}/S_L$ which remains comparable to the 1D laminar head on quenching simulation [16] with α_{T_0} being the unburned gas thermal diffusivity.) in the case of the isothermal wall, and the unburned reactants diffuse from the wall adjacent region to away from the wall, which also leads to an increase in $\widetilde{c}$ in the vicinity of the wall at the later stages of flame quenching (e.g. at $t/t_f = 14.70$), which is also consistent with several previous findings [10,15,18].

Fig. 2 shows that $\widetilde{k}$ vanishes at the wall for all time instants due to the no-slip boundary condition. Further, it can be seen from Fig. 2 that $\widetilde{k}$ increases from the wall and attains peak value before decreasing again with increasing y/h. The peak value of $\widetilde{k}$ is obtained at $y/h \approx 0.13$ (i.e. $y^+_{NR} = \rho_R u_{\tau,NR} y/\mu_R \approx 14.30$) due to the shear-generated turbulence within TBL for non-reacting as well as for FWI under both I and A wall boundary conditions. At $t/t_f = 4.20$, when the flame is away from the wall, the peak value of $\widetilde{k}$, which occurs within the unburned gas, exhibits a good agreement with the corresponding non-reacting simulation data. However, a comparison between the TKE variations in flames and the non-reacting simulation even at early stages of FWI (e.g. $t/t_f = 4.20$) reveals that $\widetilde{k}$ decreases within the flame brush. At $t/t_f = 10.50$, the peak value of $\widetilde{k}$ is still obtained close to $y/h = 0.13$, but its magnitude is smaller than the corresponding non-reacting value because the peak value of $\widetilde{k}$ occurs towards the leading edge of the flame brush. At $t/t_f = 14.70$, when the boundary layer is predominantly made up of burned gases (i.e. $\widetilde{c} \approx 1.0$), the peak magnitude of $\widetilde{k}$ is significantly smaller than the corresponding value for non-reacting flows. However, the magnitude of $\widetilde{k}$ for the reacting cases remains greater than the corresponding value in the case of non-reacting flow for $y/h > 0.5$ at $t/t_f = 10.50$, which corresponds to the middle of the flame brush where the augmentation of kinetic energy takes place due to flame-generated turbulence. Moreover, $\widetilde{k}$ for the reacting cases remains greater than the corresponding value in the case of non-reacting flow for $y/h >$ 0.8 at $t/t_f = 14.70$ even through the reacting flow TBL is predominantly made up of the burned gas at that time instant.

In order to explain the aforementioned behaviour, it is worthwhile to consider the variations of the terms on the right-hand side of the transport equation of $\widetilde{k}$ (i.e. Eq. (1)). It is worth noting that the balance of left- and right-hand sides has been assessed during the course of this analysis, and the differences in left- and right-hand sides of Eq. (1) was found to be at most 1.0% for the time instants discussed in this paper. Fig. 3 shows $[T_1, T_2, T_3, T_4, T_5, T_6] \times h/(\rho_R u^3_{\tau,NR})$ at $t/t_f = 4.20$, 10.50 and 14.70. It can be seen from Fig. 3 that T_1, and T_4 remain the dominant contributors to the TKE transport in the case of non-reacting flows, whereas T_6 assumes positive values close to the wall but becomes negative at the location where T_1 assumes the maximum value. The magnitude of T_5 remains small in comparison to those of T_1, T_4 and T_6. The terms T_2 and T_3 vanish for low Mach number non-reacting flows, as considered for the current analysis. A comparison between Figs. 2 and 3 reveals that the production of TKE by T_1 in the non-reacting flow attains the peak value close to the location where the maximum value of $\widetilde{k}$ is obtained. Moreover, the source contribution of T_1 is mostly balanced by the sink contribution of T_4 at all the time instants in the non-reacting simulation case. The TKE transport in the unburned gas for the premixed flame cases for both I and A wall boundary conditions are both qualitatively and quantitatively similar to the corresponding non-reacting simulation results at $t/t_f =$ 4.20, when the flame is away from the wall. However, mean velocity gradient term T_1 in the reacting cases assumes negative values within the flame brush, whereas this term remains positive in the non-reacting case. Moreover, the pressure dilata-

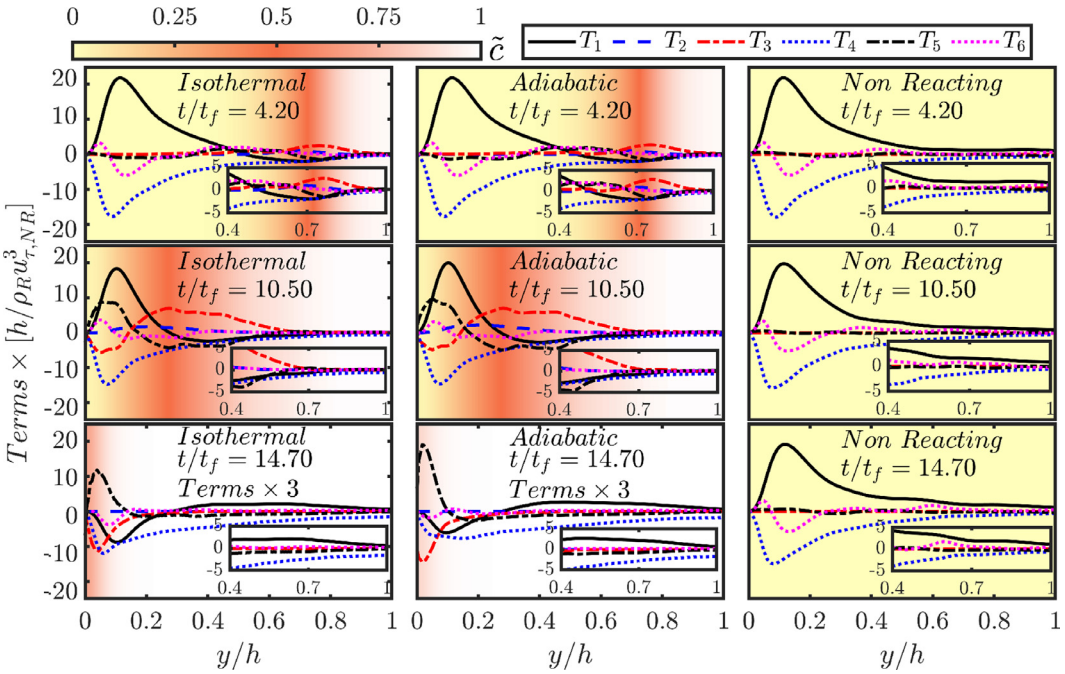

Fig. 3. Variations of $[T_1, T_2, T_3, T_4, T_5, T_6]\times h/(\rho_R u^3_{\tau,NR})$ with y/h at $t/t_f = 4.20$, 10.50, and 14.70 (note the multiplication factor) for premixed flame cases for I (left), A (middle) wall boundary conditions and the non-reacting (NR) (right) cases.

tion and pressure transport (i.e., T_3 and T_5) terms play leading order roles within the flame brush in the reacting cases, whereas these contributions are negligible in the non-reacting simulation. This statistical behaviours of the terms of the TKE transport within the flame brush when the flame is away from the wall (e.g. $t/t_f = 4.2$) are consistent with previous findings by Zhang and Rutland [9]. Note that the focus of this analysis is to analyse the differences in the TKE transport during FWI in TBLs from a conventional non-reacting TBL. Thus, the behaviours of the terms in the TKE transport equation within the flame brush and their modelling are not discussed further in this paper.

The TKE transport in the reacting cases is both qualitatively and quantitatively different at $t/t_f = 10.50$ compared to the non-reacting case when the flame is close to the wall but yet to interact with the wall for both boundary conditions. The terms T_1 and T_4 continue to remain in approximate equilibrium within the unburned gas but T_1 assumes negative value within the flame brush. Moreover, the pressure dilatation term T_3 plays a leading order role at $t/t_f = 10.50$ and assumes mostly positive value within the flame brush before vanishing on the burned gas side but negative values are obtained towards the leading edge of the flame brush close to the wall. The negative values of T_3 towards the unburned gas side of the flame brush is consistent with previous analyses [1,10]. However, this has serious modelling implications, as T_3 models proposed by Zhang and Rutland [9] and Nishiki et al. [12] only allow for positive values. The pressure transport term T_5 also plays an important role at this time instant for the reacting cases and exhibits a qualitatively opposite behaviour to that of the pressure dilatation term T_3. The behaviour of the turbulent transport term T_6 at $t/t_f = 10.50$ remains qualitatively similar to that at $t/t_f = 4.20$ in the premixed flame cases irrespective of the boundary condition. The leading order positive contribution of T_3 is responsible for the augmentation of $\widetilde{k}$ in premixed flame cases in comparison to the non-reacting case at $t/t_f = 10.50$. At $t/t_f = 14.70$, when the flames are at the advanced stage of HOI, the variations of T_5 and T_3 are opposite to each other, whereas T_1 assumes negative values close to the wall before assuming positive values away from it. The combined diffusion and dissipation term T_4 continues to have a leading order negative contribution and an approximate equilibrium is maintained between T_1 and T_4 away from the wall. Moreover, a comparison of the magnitudes of the different terms of the $\widetilde{k}$ transport equation at different time instants reveals that the leading order contributors to the $\widetilde{k}$ transport at $t/t_f = 14.70$ remain much smaller than those at $t/t_f = 4.20$ and 10.50. Moreover, there is no significant active source of $\widetilde{k}$ in the vicinity of the wall at the final stages of HOI, which is reflected in the rapid decay of $\widetilde{k}$, as the flame interacts with the wall. As the term T_4 is a combined

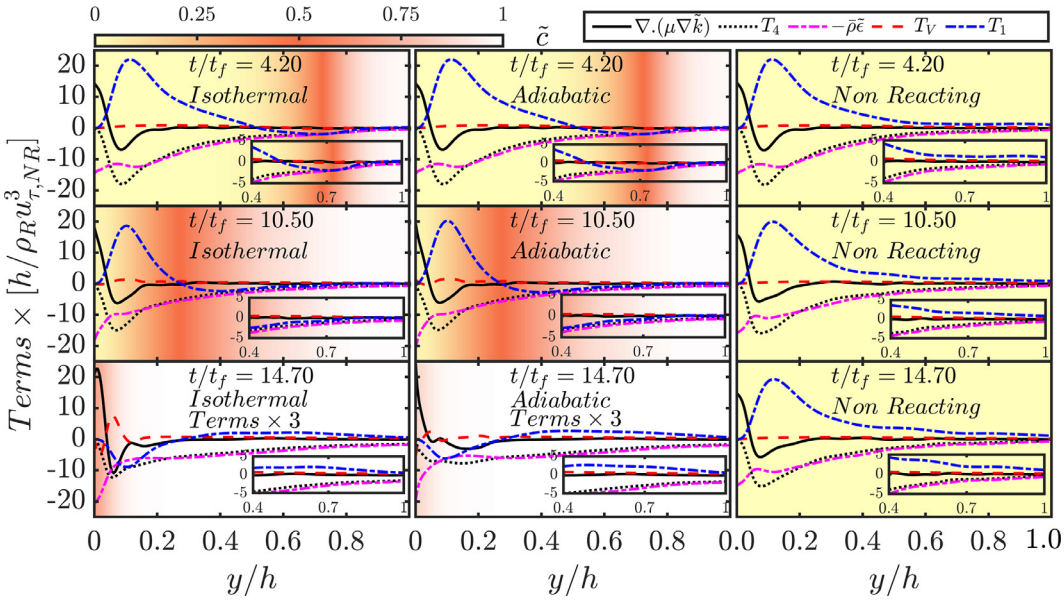

Fig. 4. Variations of $\nabla\cdot(\mu\nabla\widetilde{k})$, $(-\overline{\rho}\widetilde{\varepsilon})$, T_V, T_4 and $T_1\times h/(\rho_R u^3_{\tau,NR})$ with y/h at $t/t_f = 4.20$, 10.50, and 14.70 for HOI for I (left),A (middle) boundary conditions and NR (right) flow.

contribution of molecular diffusion and dissipation rates, it is worthwhile to analyse the behaviours of the individual contributions because the equilibrium between T_1 and T_4 is often considered for the development of wall functions [27]. The term T_4 can be split as [8,10,11]:

$$T_4 = -\overline{\rho}\widetilde{\varepsilon} + \nabla\cdot(\mu\nabla\widetilde{k}) + \underbrace{\left[\overline{u_i''\frac{\partial}{\partial x_k}\left(\mu\frac{\partial u_k''}{\partial x_i}\right)} - \frac{2}{3}\overline{u_i''\frac{\partial}{\partial x_i}\left(\mu\frac{\partial u_k''}{\partial x_k}\right)}\right]}_{T_V} \quad (2)$$

where $\widetilde{\varepsilon} = \overline{[\mu(\partial u_i''/\partial x_j)(\partial u_i''/\partial x_j)]}/\overline{\rho}$ (with μ being the dynamic viscosity) is the dissipation rate of k [12]. Fig. 4 shows the variations of individual terms of Eq. (2) along with T_1 at different time instants. Eq. (2) indicates that T_V is identically zero for low Mach number non-reacting flows where $(\partial u_i''/\partial x_i)$ vanishes. This can indeed be verified from Fig. 4 for the non-reacting flow considered here. For HOI the term T_V has a negligible magnitude in comparison to $(-\overline{\rho}\widetilde{\varepsilon})$. The magnitudes and behaviours of $(-\overline{\rho}\widetilde{\varepsilon})$ and $\nabla\cdot(\mu\nabla\widetilde{k})$ for the reacting cases are similar to the non-reacting case at $t/t_f = 4.20$ when the flame is sufficiently away from the wall, but their magnitudes decrease at the final stages of HOI (e.g. compare $t/t_f = 14.70$ with 4.20 in Fig. 4). The relative contribution of T_V to T_4 in the near-wall region increases with time, and its magnitudes become comparable to $\nabla\cdot(\mu\nabla\widetilde{k})$, which only assumes significant magnitudes for $y/h \le 0.2$. Fig. 4 shows that $(-\overline{\rho}\widetilde{\varepsilon})$ is the dominant contributor to T_4 for both reacting and non-reacting cases at all times, and the negative value of T_4 originates due to $(-\overline{\rho}\widetilde{\varepsilon})$, which assumes the highest magnitude at the wall.

The statistical behaviours of $\widetilde{\varepsilon}$ have significant implications on turbulence modelling in the context of the $k-\varepsilon$ model [1,27] and the development of wall functions [1,27] for the near-wall treatment, which will be discussed next in the paper. According to the $k-\varepsilon$ model [27] the mean velocity gradient term T_1 is modelled as: $T_{1_M} = \tau_{ij}^{k-\varepsilon}(\partial\widetilde{u}_i/\partial x_j)$, whereas $\tau_{ij}^{k-\varepsilon}$ is the modelled expression for $(-\overline{\rho u_i'' u_j''})$. According to Boussinesq's hypothesis $\tau_{ij}^{k-\varepsilon}$ is expressed as [27]: $\tau_{ij}^{k-\varepsilon} \approx 2\mu_t(\widetilde{s}_{ij} - 1/3\widetilde{s}_{kk}\delta_{ij}) - 2/3\overline{\rho}\widetilde{k}\delta_{ij}$. Here, $\widetilde{s}_{ij} = 0.5(\partial\widetilde{u}_i/\partial x_j + \partial\widetilde{u}_j/\partial x_i)$ is the component of the mean strain rate tensor and $\mu_t = \overline{\rho}C_\mu\widetilde{k}^2/\widetilde{\varepsilon}$ is the eddy viscosity with C_μ being a model parameter which is usually taken to be 0.09 in the context of the $k-\varepsilon$ model [27]. The predictions of $T_{1_M} = \tau_{ij}^{k-\varepsilon}(\partial\widetilde{u}_i/\partial x_j)$ are compared to T_1 extracted from DNS data in Fig. 5, which reveals that T_{1_M} overpredicts T_1 in the near-wall region for both reacting and non-reacting flows (note the non-reacting flow results are shown with a subscript of NR). It is worth noting that the location at which the peak value of $T_{1,NR}$ is obtained corresponds to $y^+_{NR} = 14.0$ and thus the expression $\mu_t = \overline{\rho}C_\mu\widetilde{k}^2/\widetilde{\varepsilon}$ in the context of the standard $k-\varepsilon$ model is not applicable here (because it is strictly valid for $y^+_{NR} > 40$ [27]).

Fig. 5 shows that in spite of quantitative discrepancies between $T_{1_{NR}}$ and $T_{1_{NR_M}}$ in the near-

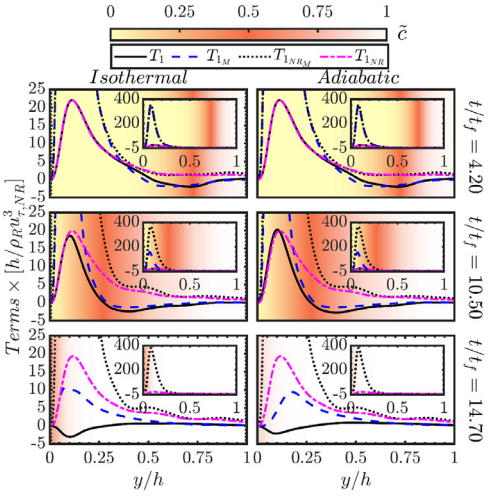

Fig. 5. Variations of the predictions of $T_{1_M} = \tau_{ij}^{k-\varepsilon}(\partial\widetilde{u}_i/\partial x_j)$ with y/h along with T_1 extracted from DNS data at $t/t_f = 4.20, 10.50$, and 14.70 for I (left) and A (right) boundary conditions.

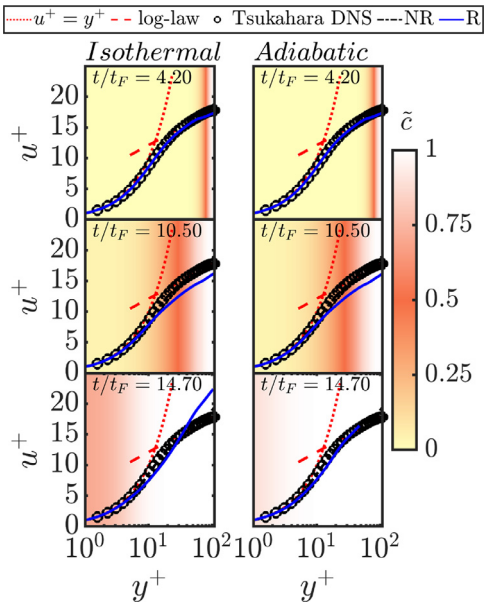

Fig. 6. Variations of $u^+ = \widetilde{u}_1/u_\tau$ with $y^+ = \rho_w u_\tau y/\mu_w$ at $t/t_f = 4.20, 10.50$, and 14.70 for I (left) and A (right) boundary conditions. Here R, represents reacting and NR, represents the non-reacting case.

wall region, these terms tend to show a reasonable quantitative agreement for $y/h > 0.37$ (or $y^+_{NR} > 40$), which is consistent with the expectations for the standard $k-\varepsilon$ model [27]. Fig. 5 further shows that T_{1NR_M} predicts a positive value, whereas locally negative values of T_1 are obtained from DNS data at $t/t_f = 10.50$ and 14.70 but at these time instants a part of the flame brush remains within $0 \le y^+ = \rho_w u_\tau y/\mu_w \le 40$ (with u_τ is the local friction velocity), where $y^+ = 40$ corresponds to $y/h = 0.38$ and 0.51 (0.40 and 1.13) at $t/t_f = 10.50$ and 14.70, respectively for I(A) wall boundary condition. This is also valid at $t/t_f = 4.20$ for the premixed flame cases even for $y^+ > 40$, which corresponds to $y/h > 0.37$. This is a consequence of counter-gradient behaviour of the Reynolds stress components $(-\overline{\rho u_i'' u_j''})$ in the reacting cases. This behaviour is consistent with previous findings [1,2,10,28] for turbulent premixed flames belonging to the corrugated flamelets regime [13] without the influence of walls. The development of new models of $(-\overline{\rho u_i'' u_j''})$ for turbulent premixed combustion in the case of FWI is beyond the scope of the current analysis but during FWI the standard Boussinesq hypothesis in the context of the $k-\varepsilon$ model is unlikely to be valid close to the wall (e.g. within the viscous sub-layer).

The standard wall functions in the context of $k-\varepsilon$ model are proposed based on the assumed equilibrium between T_1 and $(\overline{\rho}\widetilde{\varepsilon})$. Fig. 4 shows that $(-\overline{\rho}\widetilde{\varepsilon})$ assumes non-zero values at the wall, whereas T_1 is identically zero at the wall. However, $T_1 = \overline{\rho}\widetilde{\varepsilon}$ is approximately valid for the non-reacting flow simulation results for $y/h > 0.37$, which is equivalent to $y^+_{NR} > 40$ and consistent where the standard wall functions are expected to be valid. However, this equilibrium is not maintained within the flame brush at all stages of HOI because either $\overline{\rho}\widetilde{\varepsilon}$ dominates over T_1 for a major part of the TBL or both T_1 and $(-\overline{\rho}\widetilde{\varepsilon})$ assume negative values.

Under local equilibrium (i.e. $T_1 = \overline{\rho}\widetilde{\varepsilon}$) for the non-reacting constant density fully-developed channel flow one obtains: $T_{1NR_M} = \mu_t\,(\partial\widetilde{u}_1/\partial y)^2 \approx \overline{\rho}\widetilde{\varepsilon}$ upon using gradient hypothesis to model $(-\overline{\rho u_i'' u_j''})$. This yields the well-known log-law (i.e. $u^+ = \widetilde{u}_1/u_\tau = (1/\kappa)\,\ln\,(\rho u_\tau y/\mu) + B$) in the inertial layer [27] when $\mu_t = \overline{\rho} u_\tau \kappa y$ and $\widetilde{\varepsilon} = u_\tau^3/(\kappa y)$ are used with $u_\tau = \sqrt{|\tau_w|/\rho}$ and $\kappa = 0.41$ being the local friction velocity and the von-Karman's constant, respectively. However, $T_1 \approx \overline{\rho}\widetilde{\varepsilon}$ is not maintained during HOI irrespective of the thermal wall boundary condition, and therefore the log-law is not expected to be valid at the advanced stages of FWI. This can be confirmed from the variations of normalised streamwise velocity $u^+ = \widetilde{u}_1/u_\tau$ with non-dimensional wall-normal distance $y^+ = \rho_w u_\tau y/\mu_w$ presented in Fig. 6. However, the variation of u^+ with y^+ for non-reacting flow follows a log-law and agrees well with previous fully developed channel flow DNS results at $Re_\tau = 110$ by Tsukahara et al. [19]. Moreover, a reasonable agreement with the log-law is obtained for the reacting cases for both I and A wall boundary conditions at $t/t_f = 4.20$ when the flames are sufficiently away from the wall, and the TKE transport within a ma-

jor part of the TBL (including inertial layer) resembles the corresponding non-reacting flow simulation results. However, the variation of u^+ with y^+ for the premixed flame case does not follow the log-law at $t/t_f = 10.50$ for both I and A wall boundary conditions. The same is true for HOI with I wall boundary condition at $t/t_f = 14.70$, whereas the variation of u^+ with y^+ for the A boundary condition does not go beyond the buffer layer at $t/t_f = 14.70$ (e.g. the maximum value of y^+ is 47 at $t/t_f = 14.70$) and thus the log-law behaviour cannot be expected. It is worth noting that u_τ in the case of premixed HOI decreases in comparison to $u_{\tau,NR}$ due to the density change in the reacting case and the redistribution of momentum from the streamwise direction to the direction of mean flame propagation, which is also aligned with the wall normal direction in this configuration [16]. However, this drop of u_τ in comparison to $u_{\tau,NR}$ is stronger in the case of I boundary condition than in the case of A boundary condition [16] because the flame quenches away from the wall for I boundary condition, whereas it is possible to sustain chemical reaction at the wall for the A wall boundary condition and the associated thermal expansion effects lead to a reduction in density at the wall leading to higher values of u_τ. The higher value of u_τ in the case of A wall boundary condition than in the I wall boundary condition yields a smaller range of u^+ values in the case of the adiabatic wall at $t/t_f = 14.70$.

Fig. 6 suggests that the log-law based wall functions may not be valid in reacting flow TBLs during premixed FWI. Moreover, upon using Boussinesq's hypothesis one obtains $\mu_t\ (\partial\widetilde{u}_1/\partial y)^2 \approx \overline{\rho}\widetilde{\varepsilon}$ which yields $u_\tau = C_\mu^{1/4}\sqrt{\widetilde{k}}$ and $\widetilde{\varepsilon} = C_\mu^{3/4}\widetilde{k}^{3/2}/(\kappa y)$, that are used as wall functions within the inertial layer (i.e. $y^+_{NR} > 40$) for non-reacting flows [27]. However, it has been found from the results shown in Fig. 5 that the modelling of T_1 by using Boussinesq's (i.e gradient) hypothesis may not remain valid during premixed FWI in TBLs. Thus, the standard wall functions might not yield accurate predictions in the context of standard $k-\varepsilon$ modelling of premixed FWI in TBLs. This necessitates the development of new wall functions for premixed FWI in TBLs.

5. Conclusions

The statistical behaviours of the distribution and transport of $\widetilde{k}$ in HOI of premixed flames with chemically inert walls have been investigated for $Re_\tau = 110$ using DNS data for both isothermal and adiabatic wall boundary conditions. The wall-normal distributions of $\widetilde{k}$, its dissipation rate and different unclosed terms in its transport equation in the unburned gas region of the reacting flow TBL resemble the corresponding non-reacting constant density simulation in the same configuration when the flame is away from the wall for both isothermal and adiabatic wall boundary conditions. The mean velocity gradient and dissipation terms have been found to be leading order contributors to $\widetilde{k}$ transport when the flame remains away from the wall but in addition to these terms both pressure dilatation and pressure transport terms play significant roles in the $\widetilde{k}$ transport when the flame comes in the vicinity of the wall. The magnitudes of $\widetilde{k}$ and the unclosed terms of its transport equation decrease at the final stages of HOI. Boussinesq's hypothesis (i.e. gradient hypothesis) based Reynolds stress closure using the eddy viscosity evaluated in terms of $k-\varepsilon$ model does not adequately capture the behaviour of T_1 in the turbulent premixed flame cases considered here where the Reynolds stresses locally exhibit counter-gradient behaviour. The local equilibrium between the production and dissipation rates of $\widetilde{k}$ is not maintained at advanced stages of turbulent premixed FWI. Thus, the usual log-law expression for the mean streamwise velocity variation within the TBLs and the associated wall functions in the framework of standard $k-\varepsilon$ model are rendered invalid for premixed FWI. Therefore, the development of new wall functions for premixed FWI in TBLs, which are not dependent on conventional log-law for non-reacting TBLs, will be necessary. Moreover, further analyses with higher values of Re_τ and detailed chemistry will be necessary to validate the findings of the present analysis.

Declaration of Competing Interest

The authors declare that they have no known competing financial interests or personal relationships that could have appeared to influence the work reported in this paper.

Acknowledgments

The authors are grateful for the support from EPSRC (EP/V003534/1, EP/R029369/1), SuperMUC-NG (pn69ga, pn34xu), and ROCKET HPC facility at Newcastle University.

Supplementary material

The results for $t/t_f = 12.60$ are shown in the supplementary material.

Supplementary material associated with this article can be found, in the online version, at doi:10.1016/j.proci.2022.08.055.

References

[1] U. Ahmed, A.L. Pillai, N. Chakraborty, R. Kurose, Statistical behavior of turbulent kinetic energy transport in boundary layer flashback of hydrogen-rich premixed combustion, Phys. Rev. Fluids 4 (2019).

[2] J. Lai, A. Moody, N. Chakraborty, Turbulent kinetic energy transport in head-on quenching of turbulent premixed flames in the context of Reynolds Averaged Navier Stokes simulations, Fuel 199 (2017) 456–477.
[3] W.P. Jones, B.E. Launder, The prediction of laminarization with a two-equation model of turbulence, Int. J. Heat Mass Transf. 15 (1972) 301–314.
[4] B. Karlovitz, D.W. Denniston, D.H. Knapschaefer, F.E. Wells, Studies on turbulent flames. a. flame propagation across velocity gradients B. turbulence measurement in flames, Symp. Combust. 4 (1) (1953) 613–620.
[5] K.N. Bray, P.A. Libby, Interaction effects in turbulent premixed flames, Phys. Fluids 19 (1976) 1687–1701.
[6] P. Moreau, A. Boutier, Laser velocimeter measurements in a turbulent flame, Symp. Combust. 16 (1977) 1747–1756.
[7] R. Borghi, D. Escudie, Assessment of a theoretical model of turbulent combustion by comparison with a simple experiment, Combust. Flame 56 (1984) 149–164.
[8] J. Chomiak, J.R. Nisbet, Modeling variable density effects in turbulent flames-some basic considerations, Combust. Flame 102 (1995) 371–386.
[9] S. Zhang, C.J. Rutland, Premixed flame effects on turbulence and pressure-related terms, Combust. Flame 102 (1995) 447–461.
[10] N. Chakraborty, M. Katragadda, R.S. Cant, Statistics and modelling of turbulent kinetic energy transport in different regimes of premixed combustion, Flow, Turbul. Combust. 87 (2011) 205–235.
[11] N. Chakraborty, M. Katragadda, R.S. Cant, Effects of lewis number on turbulent kinetic energy transport in premixed flames, Phys. Fluids 23 (2011).
[12] S. Nishiki, T. Hasegawa, R. Borghi, R. Himeno, Modeling of flame-generated turbulence based on direct numerical simulation databases, Proc. Combust. Inst. 29 (2002) 2017–2022.
[13] N. Peters, Turbulent combustion, Cambridge University Press, 2000.
[14] J. Lai, M. Klein, N. Chakraborty, Direct numerical simulation of head-On quenching of statistically planar turbulent premixed methane-air flames using a detailed chemical mechanism, Flow, Turbul. Combust. 101 (2018) 1073–1091.
[15] U. Ahmed, N.A.K. Doan, J. Lai, M. Klein, N. Chakraborty, N. Swaminathan, Multiscale analysis of head-on quenching premixed turbulent flames, Phys. Fluids 30 (2018).
[16] U. Ahmed, N. Chakraborty, M. Klein, Influence of thermal wall boundary condition on scalar statistics during flame-wall interaction of premixed combustion in turbulent boundary layers, Int. J. Heat Fluid Flow 92 (2021) 108881.
[17] G. Bruneaux, K. Akselvoll, T. Poinsot, J.H. Ferziger, Flame-wall interaction simulation in a turbulent channel flow, Combust. Flame 107 (1996) 27–36.
[18] G. Bruneaux, T. Poinsot, J.H. Ferziger, Premixed flame-wall interaction in a turbulent channel flow: budget for the flame surface density evolution equation and modelling, J. Fluid Mech. 349 (1997) 191–219.
[19] T. Tsukahara, Y. Seki, H. Kawamura, D. Tochio, DNS of turbulent channel flow at very low Reynolds numbers, in: Proceedings of the 4th International Symposium on Turbulence and Shear Flow Phenomena, volume 3, 2005, pp. 935–940.
[20] U. Ahmed, N. Chakraborty, M. Klein, Assessment of Bray Moss Libby formulation for premixed flame-wall interaction within turbulent boundary layers: influence of flow configuration, Combust. Flame 233 (2021) 111575.
[21] U. Ahmed, D. Apsley, T. Stallard, P. Stansby, I. Afgan, Turbulent length scales and budgets of Reynolds stress-transport for open-channel flows; friction Reynolds numbers $\mathrm{Re}_\tau = 150, 400$ and 1020, J. Hydraul. Res. 59 (2021) 36–50.
[22] A. Gruber, R. Sankaran, E.R. Hawkes, J.H. Chen, Turbulent flame-wall interaction: a direct numerical simulation study, J. Fluid Mech. 658 (2010) 5–32.
[23] A. Gruber, J.H. Chen, D. Valiev, C.K. Law, Direct numerical simulation of premixed flame boundary layer flashback in turbulent channel flow, J. Fluid Mech. 709 (2012) 516–542.
[24] C.S. Yoo, H.G. Im, Characteristic boundary conditions for simulations of compressible reacting flows with multi-dimensional, viscous and reaction effects, Combust. Theory Model. 11 (2007) 259–286.
[25] W.D. Smyth, Dissipation-range geometry and scalar spectra in sheared stratified turbulence, J. Fluid Mech. 401 (1999) 209–242.
[26] W.D. Smyth, J.N. Moum, Anisotropy of turbulence in stably stratified mixing layers, Phys. Fluids 12 (6) (2000) 1343–1362.
[27] P.A. Durbin, B.A. Reif, Statistical Theory and Modeling for Turbulent Flows: Second Edition, John Wiley & Sons, Ltd, 2010.
[28] N. Chakraborty, Influence of thermal expansion on fluid dynamics of turbulent premixed combustion and its modelling implications, Flow, Turbul. Combust. 106 (2021) 753–848.